Digital Restoration of Multichannel Images

NIKOLAS P. GALATSANOS, STUDENT MEMBER, IEEE, AND ROLAND T. CHIN, MEMBER, IEEE

Abstract—**Digital image restoration of monochrome images has been studied extensively. However, problems associated with the restoration of multichannel images still require investigation. In this paper, the Wiener solution of a multichannel restoration scheme is presented. Using matrix diagonalization and block-Toeplitz to block-circulant approximation, the inversion of the multichannel, linear space-invariant imaging system becomes feasible by utilizing a fast iterative matrix inversion procedure. The restoration uses both the within-channel (spatial) and between-channel (spectral) correlation; hence, the restored result is a better estimate than that produced by independent channel restoration. Simulations are also presented.**

I. Introduction

THE use of image data from multiple frequency bands, multiple time frames, multiple colors, or multiple sensors (e.g., optical, radar, range, etc.) can be of tremendous value in a number of applications, such as multispectral image analysis, robot vision, and satellite remote sensing. Examples include the restoration of multispectral satellite images and the enhancement of color images. For the purpose of discussion, we shall use the term *multichannel images* in general throughout this paper to imply the fact that we are dealing with multiple image planes (channels) obtained by an imaging system that measures the same scene using more than one type of sensor.

Restoration is often performed on multichannel images of a scene in order to enhance salient features or remove degradation effects to assist in subsequent human or machine analysis. Most of the restoration techniques involve individual image plane restoration without using the joint processing of multichannel image planes. An example of this type of technique is the restoration of color images by individual monochrome processing in which each color is treated separately. This is not desirable because it fails to utilize the related information between channels.

In [1], Hunt and Kübler present a multichannel restoration scheme based on the assumption that the signal autocorrelation, describing the between-channel (or spectral) and within-channel (or spatial) relationship, is separable. This enables the formulation of a linear transformation to decorrelate the signal between image channels. In other words, this transformation makes the channels orthogonal. It follows that multichannel restoration of the transformed signal is equivalent to the application of restoration to individual channels independently, and the process does not lose any between-channel information.

In this paper we describe a computationally feasible algorithm that utilizes the advantage of the special structure of the correlation matrix of the multichannel image without using the assumption of spectral and spatial separability. It uses the block-circulant to block-Toeplitz approximation, and hence the discrete Fourier transform (DFT).

Section II describes the image formation model and establishes the necessary mathematical notations. Independent restoration of individual images is reviewed in this section. Section III presents the multichannel restoration algorithm. Section IV presents experimental results.

II. The Image Formation Model

A linear shift-invariant monochrome imaging system can be modeled by

$$g(x, y) = \int_{-\infty}^{+\infty} \int_{-\infty}^{+\infty} f(x', y')\, h(x - x', y - y') \cdot dx'\, dy' + n(x, y) \tag{2-1}$$

where $f(x, y)$ is the unknown ideal image, $g(x, y)$ is the known observed image, $h(x, y)$ is the degradation function, and $n(x, y)$ is a noise process that is uncorrelated to $f(x, y)$. The discrete version of this system is a set of linear equations

$$g(j, k) = \sum_{m=0}^{M-1} \sum_{n=0}^{M-1} f(m, n)\, h(j - m, k - n) + n(j, k) \tag{2-2}$$

and they can be represented by matrix notation as

$$g = Hf + n \tag{2-3}$$

where f, g, and n are lexicographic orders, by either column or row, of the two-dimensional image of size $M \times M$ into one-dimensional vectors of length M^2. The matrix H is the discrete representation of the degradation of dimension $M^2 \times M^2$. For linear shift-invariant systems, matrix H is block Toeplitz, that is, H is partitioned in blocks and each block is Toeplitz; see [3].

For a multichannel imaging system with N channels each of size $M \times M$, the imaging model becomes

$$g_i = H_i f_i + n_i \quad \text{for } i = 1, 2, \cdots, N \tag{2-4}$$

Manuscript received June 24, 1987; revised June 26, 1988. This work was supported by the National Science Foundation under Grant ECS-8352356 and ATM-8414467, and in part by NASA under Grant NAG 5-580.

The authors are with the Department of Electrical and Computer Engineering, University of Wisconsin, Madison, WI 53706.

IEEE Log Number 8825666.

where g_i, f_i, n_i, and H_i are the observed image, the ideal image, the noise, and the degradation function of the ith channel, respectively.

Equation (2-4) can be further simplified by adopting the following notation:

$$\boldsymbol{g} = \begin{bmatrix} g_1 \\ g_2 \\ \vdots \\ g_N \end{bmatrix}; \quad \boldsymbol{f} = \begin{bmatrix} f_1 \\ f_2 \\ \vdots \\ f_N \end{bmatrix}; \quad \boldsymbol{n} = \begin{bmatrix} n_1 \\ n_2 \\ \vdots \\ h_N \end{bmatrix} \tag{2-5}$$

where $\boldsymbol{g}, \boldsymbol{f}$, and $\boldsymbol{n}$ are $N \times M^2$ in length. The degradation $\boldsymbol{H}$ of the multichannel image is

$$\boldsymbol{H} = \begin{bmatrix} H_1 & 0 & \cdots & 0 \\ 0 & H_2 & \cdots & 0 \\ \vdots & 0 & \cdots & 0 \\ & \vdots & \cdots & \vdots \\ 0 & 0 & \cdots & H_N \end{bmatrix} \tag{2-6}$$

and is of dimension $NM^2 \times NM^2$. Finally, the multichannel imaging equation can be written as

$$\boldsymbol{g} = \boldsymbol{Hf} + \boldsymbol{n}. \tag{2-7}$$

The linear minimum mean square error (LMMSE) solution to (2-7) is the well-known Wiener solution, given by

$$\hat{\boldsymbol{f}} = \boldsymbol{R}_f \boldsymbol{H}^t [\boldsymbol{H} \boldsymbol{R}_f \boldsymbol{H}^t + \boldsymbol{R}_n]^{-1} \boldsymbol{g} \tag{2-8}$$

where $\hat{\boldsymbol{f}}$ is the estimate of $\boldsymbol{f}$, and $\boldsymbol{R}_f$ and $\boldsymbol{R}_n$ are the autocorrelation of the multichannel signal and the noise, respectively. The solution requires the inversion of

$$\bar{\boldsymbol{R}} = [\boldsymbol{H} \boldsymbol{R}_f \boldsymbol{H}^t + \boldsymbol{R}_n]. \tag{2-9}$$

Let us further examine $\boldsymbol{R}_f$ and $\boldsymbol{R}_n$. Let $R_f^{il} = E[f_i f_l^t]$ be the correlation between channel i and l. Then

$$\boldsymbol{R}_f = \begin{bmatrix} R_f^{11} & R_f^{12} & & R_f^{1N} \\ R_f^{21} & R_f^{22} & & R_f^{2N} \\ \vdots & \vdots & \vdots & \vdots \\ R_f^{N1} & \boldsymbol{R}_f^{N2} & & R_f^{NN} \end{bmatrix} \tag{2-10}$$

is an $NM^2 \times NM^2$ matrix.

The autocorrelation matrix of $\boldsymbol{n}$, $\boldsymbol{R}_n$, is defined in (2-11) by assuming that the between-channel noise is uncorrelated; that is, $R_n^{il} = 0$ for $i \neq l$. Using the definition $R_n^{il} = E[n_i n_l^t]$, we have

$$\boldsymbol{R}_n = \begin{bmatrix} R_n^{11} & 0 & \cdots & 0 \\ 0 & R_n^{22} & \cdots & 0 \\ \vdots & \vdots & \cdots & \vdots \\ 0 & 0 & \cdots & R_n^{NN} \end{bmatrix}. \tag{2-11}$$

If white noise is assumed for $\boldsymbol{n}$, then $R_n^{ii} = \sigma_{ii}^2 I$, where σ_{ii}^2 is the variance of n_i.

Using (2-9), (2-10), and (2-11),

$$\bar{\boldsymbol{R}} = \begin{bmatrix} H_1 R_f^{11} H_1^t + R_n^{11} & H_1 R_f^{12} H_2^t & & H_1 R_f^{1N} H_N^t \\ H_2 R_f^{21} H_1^t & H_2 R_f^{22} H_2^t + R_n^{22} & & H_2 R_f^{2N} H_N^t \\ \vdots & \vdots & \vdots & \vdots \\ H_N R_f^{N1} H_1^t & H_N R_f^{N2} H_2^t & & H_N R_f^{NN} H_N^t + R_n^{NN} \end{bmatrix} \tag{2-12}$$

and it is of dimension $NM^2 \times NM^2$

For any realistic application, for example, $M = 128$ and $N = 3$, the direct computation of (2-8) is not practical, requiring the inversion of a 49 152 × 49 152 matrix.

A. Independent Restoration of Image Planes

Block-Toeplitz to block-circulant approximation has been used in monochrome image restoration to enable the inversion of the imaging system using DFT. For stationary and linear shift-invariant images, the signal autocorrelation and the system degradation matrices are block Toeplitz, each of dimension $M^2 \times M^2$. Using the block-Toeplitz to block-circulant approximation and the fact that circulant matrices have identical eigenvectors, the Wiener solution of the monochrome image restoration is reduced to a set of scalar equations in the Fourier domain via the two-dimensional DFT; see [3]. Hence, inverting the imaging system is feasible and straightforward. The validity of the block-Toeplitz to block-circulant approximation has been verified [4] and it has been shown that as the dimension of the matrix grows, a block-Toeplitz matrix is asymptotically equivalent to a block-circulant matrix in the Euclidean norm sense.

In examining (2-8), the multichannel inversion formulation, one can see that the noise autocorrelation $\boldsymbol{R}_n$ for a white noise process is block diagonal. The autocorrelation matrix $\boldsymbol{R}_f$ of the multispectral vector $\boldsymbol{f}$ given by (2-10) is not block Toeplitz but it can be partitioned into submatrices that are block Toeplitz. If we assume that $R_f^{il} = 0$ for $i \neq l$, that is, image channels are uncorrelated, then from (2-10) we obtain

$$\boldsymbol{R}_f = \begin{bmatrix} R_f^{11} & 0 & \cdots & 0 \\ 0 & R_f^{22} & \cdots & 0 \\ \vdots & \vdots & \vdots & \vdots \\ 0 & 0 & \cdots & R_f^{NN} \end{bmatrix}. \tag{2-13}$$

Using this assumption, the inversion formulation of (2-8) becomes

$$\hat{f}_i = R_f^{ii} H_i^t [H_i R_f^{ii} H_i^t + R_n^{ii}]^{-1} g_i \qquad i = 1, 2, \cdots, N \tag{2-14}$$

which represents the independent channel restoration approach with the implicit assumption that the correlation between channels is zero. Since this assumption is not valid for multichannel images, it is clear that the independent channel restoration is a suboptimal solution to the true multichannel restoration because it fails to include information on the joint spatial and spectral correlations of the multichannel imaging system.

III. The Multichannel Image Restoration Algorithm

In multichannel image restoration, the signal correlation matrix $\boldsymbol{R}_f$ given by (2-10) is not block Toeplitz. The elements of $\boldsymbol{R}_f$, R_f^{il}, are block Toeplitz for stationary images but they are not arranged in a Toeplitz order because

$$R_f^{il} \neq R_f^{i+k,l+k} \qquad k = 1, 2, \cdots.$$

This can be explained by the fact that different channels embody different properties of the scene being imaged, and these differences can lead to substantial differences between the image pair (i, l) and $(i + k, l + k)$, and therefore there is no justification to assume stationarity between channels. Not being able to assume block Toeplitz for $\boldsymbol{R}_f$, Fourier domain computations cannot be used directly to decompose (2-8).

The algorithm presented below overcomes the above stated problem and allows the computation of $\hat{\boldsymbol{f}}$ efficiently from (2-8) without requiring the usage of Hunt and Kübler's separability assumption [1] and the between-channel stationarity assumption.

Let us first define the DFT operation. The DFT of an $M \times M$ signal $f(m, n)$ is defined by

$$F(u, v) = \sum_{m=0}^{M-1} \sum_{n=0}^{M-1} f(m, n) \exp\left[-j \frac{2\pi}{M} (um + vn)\right]$$

for

$$u, v = 0, 1, 2, \cdots, M - 1$$

and it can be also written in vector matrix notation as

$$F = \boldsymbol{W}^{-1} f \tag{3-1}$$

where F and f are lexicographic orders of $F(u, v)$ and $f(m, n)$, respectively, and are of length M^2. The matrix $\boldsymbol{W}^{-1}$ contains the complex exponentials and is of dimension $M^2 \times M^2$. See [2] for a more detailed description of this representation.

Similarly, the inverse is

$$f = \boldsymbol{W} F$$

where $\boldsymbol{W}$ is defined accordingly; see [2].

In [2] it has been shown that for a block-circulant matrix C of dimension $M^2 \times M^2$ given by

$$C = \begin{bmatrix} [c]_1 & [c]_M & \cdots & [c]_2 \\ [c]_2 & [c]_1 & \cdots & [c]_3 \\ \vdots & \vdots & \vdots & \vdots \\ [c]_M & [c]_{M-1} & \cdots & [c]_1 \end{bmatrix}$$

where $[c]_j$ are $M \times M$ circulant matrices given by

$$[c]_j = \begin{bmatrix} c_j^1 & c_j^M & \cdots & c_j^2 \\ c_j^2 & c_j^1 & \cdots & c_j^3 \\ \vdots & \vdots & \vdots & \vdots \\ c_j^M & c_j^{M-1} & \cdots & c_j^1 \end{bmatrix}$$

the following is true:

$$D = \boldsymbol{W}^{-1} C \boldsymbol{W} \tag{3-2}$$

where D is an $M^2 \times M^2$ diagonal matrix.

Equation (3-2) represents the diagonalization of a block-circulant matrix via the 2-D DFT. Having established the above, we proceed with the description of the multichannel restoration algorithm.

Let us define an $NM^2 \times NM^2$ transformation matrix $\overline{\boldsymbol{W}}$ as

$$\overline{\boldsymbol{W}} = \begin{bmatrix} \boldsymbol{W} & 0 & \cdots & 0 \\ 0 & \boldsymbol{W} & \cdots & 0 \\ \vdots & \vdots & \vdots & \vdots \\ 0 & 0 & \cdots & \boldsymbol{W} \end{bmatrix} \tag{3-3}$$

where $\boldsymbol{W}$ satisfies (3-2). The matrix inverse, $\overline{\boldsymbol{W}}^{-1}$, is then given by

$$\overline{\boldsymbol{W}}^{-1} = \begin{bmatrix} \boldsymbol{W}^{-1} & 0 & \cdots & 0 \\ 0 & \boldsymbol{W}^{-1} & \cdots & 0 \\ \vdots & \vdots & \vdots & \vdots \\ 0 & 0 & \cdots & \boldsymbol{W}^{-1} \end{bmatrix}. \tag{3-4}$$

Applying $\overline{\boldsymbol{W}}^{-1}$ to (2-8) we obtain

$$\overline{\boldsymbol{W}}^{-1} \hat{\boldsymbol{f}} = [\overline{\boldsymbol{W}}^{-1} \boldsymbol{R}_f \overline{\boldsymbol{W}}] [\overline{\boldsymbol{W}}^{-1} \boldsymbol{H}^t \overline{\boldsymbol{W}}] \cdot [\overline{\boldsymbol{W}}^{-1} [\boldsymbol{H} \boldsymbol{R}_f \boldsymbol{H}^t + \boldsymbol{R}_n] \overline{\boldsymbol{W}}]^{-1} \overline{\boldsymbol{W}}^{-1} \boldsymbol{g}. \tag{3-5}$$

The term $\overline{\boldsymbol{W}}^{-1} \boldsymbol{g}$ is the DFT of the observed N-channel image, and $\overline{\boldsymbol{W}}^{-1} \hat{\boldsymbol{f}}$ is the DFT of the restored multichannel image.

Equation (3-5) can now be written as

$$\hat{\boldsymbol{F}} = [\overline{\boldsymbol{W}}^{-1} \boldsymbol{R}_f \overline{\boldsymbol{W}}] [\overline{\boldsymbol{W}}^{-1} \boldsymbol{H}^t \overline{\boldsymbol{W}}] \cdot [\overline{\boldsymbol{W}}^{-1} [\boldsymbol{H} \boldsymbol{R}_f \boldsymbol{H}^t + \boldsymbol{R}_n] \overline{\boldsymbol{W}}]^{-1} \overline{\boldsymbol{W}}^{-1} \boldsymbol{G} \tag{3-6}$$

where $\boldsymbol{G}$ and $\hat{\boldsymbol{F}}$ are the DFT of $\boldsymbol{g}$ and $\hat{\boldsymbol{f}}$, respectively.

Examining the elements in (3-6) separately, we have

$$\overline{W}^{-1}R_f\overline{W} = \begin{bmatrix} \overline{W}^{-1}R_f^{11}W & W^{-1}R_f^{12}W & \\ \overline{W}^{-1}R_f^{21}W & W^{-1}R_f^{22}W & \\ \vdots & \vdots & \vdots \end{bmatrix} \quad (3\text{-}7)$$

and

$$\overline{W}^{-1}H^t\overline{W} = \begin{bmatrix} W^{-1}H_1^tW & 0 & \\ 0 & W^{-1}H_2^tW & \\ \vdots & \vdots & \vdots \end{bmatrix}. \quad (3\text{-}8)$$

The last part of (3-6) is

$$\overline{W}^{-1}[HR_fH^t + R_n]\overline{W} = \begin{bmatrix} W^{-1}[H_1R_f^{11}H_1^t + R_n^{11}]W & W^{-1}[H_1R_f^{12}H_2^t]W & \\ W^{-1}[H_2R_f^{21}H_1^t]W & W^{-1}[H_2R_f^{22}H_2^t + R_n^{22}]W & \\ \vdots & \vdots & \vdots \end{bmatrix}. \quad (3\text{-}9)$$

Assuming stationary images and linear shift-invariant systems, R's and H's in the above equation are block-Toeplitz matrices. Using block-Toeplitz to block-circulant approximation and the diagonalization as defined in (3-2), equations (3-7), (3-8), and (3-9) yield block matrices with partitions that are diagonal as shown in the following:

$$\begin{bmatrix} [\bullet] & [\bullet] & \cdots & [\bullet] \\ [\bullet] & [\bullet] & \cdots & [\bullet] \\ \vdots & \vdots & \vdots & \vdots \\ [\bullet] & [\bullet] & \cdots & [\bullet] \end{bmatrix} \quad \text{(Form A)}$$

where $[\bullet]$ are $M^2 \times M^2$ diagonal matrices. Operations on matrices of this form are computationally efficient because they contain only a few nonzero elements. The following describes a computationally feasible algorithm for the inversion of such matrices.

Lemma 1: Operations (addition, subtraction, multiplication, and inversion) on Form A matrices result in Form A matrices.

Lemma 2: Any $iM^2 \times iM^2$ block matrix B_i can be partitioned as

$$B_i = \begin{bmatrix} B_{i-1} & X_{i-1} \\ Z_{i-1}^t & Y_{i-1} \end{bmatrix}$$

where B_{i-1} is an $(i-1)M^2 \times (i-1)M^2$ block matrix, X_{i-1} is a block column of dimension $(i-1)M^2 \times M^2$, Z_{i-1}^t is a block row of dimension $M^2 \times (i-1)M^2$, and Y_{i-1} is an $M^2 \times M^2$ matrix.

The inverse matrix B_i^{-1} can be determined by [5]

$$B_i^{-1} = \begin{bmatrix} B_{i-1} & X_{i-1} \\ Z_{i-1}^t & Y_{i-1} \end{bmatrix}^{-1} = \begin{bmatrix} B_{i-1}^{-1} + Q_{i-1}\alpha_{i-1}^{-1}U_{i-1}^t & Q_{i-1}\alpha_{i-1}^{-1} \\ \alpha_{i-1}^{-1}U_{i-1}^t & \alpha_{i-1}^{-1} \end{bmatrix} \quad (3\text{-}10)$$

where

$$\alpha_{i-1} = Y_{i-1} + Z_{i-1}Q_{i-1} = Y_{i-1} + U_{i-1}^tX_{i-1} \quad (3\text{-}11)$$

$$Q_{i-1} = -B_{i-1}^{-1}X_{i-1} \quad (3\text{-}12)$$

and

$$U_{i-1}^t = -Z_{i-1}^tB_{i-1}^{-1}. \quad (3\text{-}13)$$

If B_i is a Form A matrix, that is, all i^2 entries are $M^2 \times M^2$ diagonal matrices, then the above matrix inversion procedure [(3-10)–(3-13)] involves operations only with diagonal matrices, enabling the inversion to be implemented efficiently.

We have already shown that the restoration of multichannel image as formulated in (3-6) involves operations on Form A matrices given by (3-7)–(3-9). The matrix defined in (3-9) is positive definite and well conditioned. In conjunction with Lemma 2, solving for the Wiener solution of the multichannel imaging system becomes feasible. The following summarizes the restoration procedure.

Step 1: Diagonalize R_f^{il} and H_i by the transformation W for $i, l = 1, 2, \cdots, N$.

Step 2: Transform g_i by $G_i = W^{-1}g_i$ for $i = 1, 2, \cdots, N$ and construct G.

Step 3: Partition the matrix $[W^{-1}[HR_fH^t + R_n]\overline{W}]$ into N^2 partitions and use the iterative procedure (as stated by Lemma 2) $N - 1$ times to solve for the inverse.

Step 4: Solve for $\hat{F}$, the Weiner solution, as in (3-6).

Step 5: Inverse DFT of $\hat{F}$ for the restored image $\hat{f}$.

IV. Experiments

Simulations were performed to test the multichannel LMMSE restoration algorithm. Test images of dimension $128 \times 128 \times 3$ were used.

The Toeplitz-to-circulant approximation was done using the DFT. The Toeplitz matrix is first transformed by a similar transformation and then the off-diagonal elements were set to zero.

In most image restoration schemes, images stationarity is assumed; that is, the local mean and local variance are independent of the spatial position. The LMMSE restoration uses this assumption in order to become computa-

tionally feasible via the DFT. The multichannel LMMSE scheme we present here also makes use of this assumption.

In view of this, the proposed algorithm was first tested by using synthetically generated textural images which are stationary in nature. A 3 × 3 moving average process given below was used to create multichannel textural patterns $\boldsymbol{f}$.

$$\begin{aligned} f_l(j, k) = {} & a(1) \cdot w(j-2, k-2) + a(2) \\ & \cdot w(j-2, k-1) + a(3) \cdot w(j-2, k) \\ & + a(4) \cdot w(j-1, k-2) + a(5) \\ & \cdot w(j-1, k-1) + a(6) \cdot w(j-1, k) \\ & + a(7) \cdot w(j, k-2) + a(8) \\ & \cdot w(j, k-1) + a(9) \cdot w(j, k) \end{aligned} \tag{4-1}$$

where $f_l(j, k)$ is the textural image in channel l at spatial location (j, k), $w(j, k)$ is independent white Gaussian noise with zero mean and unit variance driving the model, and $a(\cdot)$ are the moving average coefficients.

Independent additive white Gaussian noise, $\boldsymbol{n}$, was added to each channel separately. Low-pass averaging filters, $\boldsymbol{H}$, implemented as 5 × 5 weighted convolution masks, were applied to degrade the channels generating the multichannel images $\boldsymbol{g}$. See Fig. 1 for the image formation model of this experiment.

The multichannel correlation was estimated by

$$R_f^{il}(j, k) = \frac{1}{M^2} \sum_{n=1}^{M} \sum_{m=1}^{M} f_i(j+n, k+m) f_l(n, m) \tag{4-2}$$

where $M = 3$ and $R_f^{il}(j, k)$ is the correlation at spatial location (j, k) between channels i and l. The signals f_i and f_l are the original image of channel i and channel l, respectively. Note that in this experiment, the correlation was estimated directly from the ideal image signal $\boldsymbol{f}$. The estimated correlation was then used in (2-12) for the restoration. To permit comparison of the performance of the multichannel restoration scheme to that of independent restoration, mean-square error (MSE) between f_i and $\hat{f}_i$ was used.

Three sets of multichannel textural images were generated, each with three channels. One of the image sets represents a strong between-channel correlation, another represents a moderate correlation, and the last set represents a weak between-channel correlation. The values of the moving average coefficients for the generation of these three sets of images are listed in Table I. The textural images were restored by the multichannel scheme, and their MSE measures are shown in Table II. As expected, the multichannel restoration outperformed the independent restoration. Furthermore, the improvement is substantial when the between-channel correlation is strong. This can easily be explained by the fact that the multichannel restoration scheme utilizes information contained in all the channels. When the between-channel correlation is weak, the performance of the multichannel scheme and the independent restoration are basically identical, because there is very little information from the other channels to be utilized.

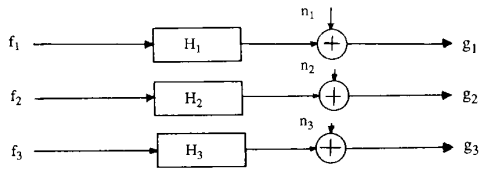

Fig. 1. The image formation model for restoration of stationary images.

TABLE I
MOVING AVERAGE COEFFICIENTS OF THE SYNTHETICALLY GENERATED TEXTURE IMAGES

	a(1)	a(2)	a(3)	a(4)	a(5)	a(6)	a(7)	a(8)	a(9)
Strong Between-Channel Correlation									
Channel 1	10	0	0	0	10	0	0	0	10
Channel 2	10	0	0	0	10	0	0	0	10
Channel 3	10	0	0	0	10	0	0	0	10
Moderate Between-Channel Correlation									
Channel 1	10	0	0	0	10	0	0	0	10
Channel 2	10	10	0	0	10	0	0	0	0
Channel 3	0	0	0	0	10	0	0	10	10
Weak Between-Channel Correlation									
Channel 1	10	0	0	0	10	0	0	0	10
Channel 2	0	10	0	0	10	0	0	10	0
Channel 3	0	0	0	10	10	10	0	0	0

TABLE II
RESTORATION OF SYNTHETICALLY GENERATED STATIONARY IMAGES. THE SNR IS 30 dB

Mean-Square Error	Channel 1	Channel 2	Channel 3
Strong Between-Channel Correlation			
Without Restoration	15.88	15.90	15.89
Independent	12.14	12.13	11.12
Multichannel	7.44	7.44	7.44
Moderate Between-Channel Correlation			
Without Restoration	15.93	13.37	13.38
Independent	11.84	9.71	9.67
Multichannel	10.82	8.98	8.93
Weak Between-Channel Correlation			
Without Restoration	16.02	15.94	15.75
Independent	8.94	11.79	8.72
Multichannel	8.36	11.51	8.21

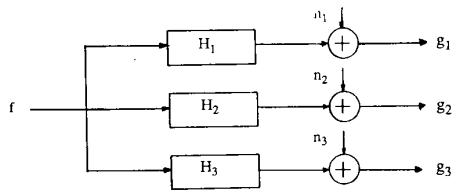

Fig. 2. The image formation model for restoration of real images.

In another experiment real images were used, as shown in Fig. 3. The image was digitized and degraded by three different low-pass filters implemented as 5 × 5, 7 × 7, and 9 × 9 convolution operators. Independent white Gaussian noise was added to each channel. See Fig. 2 for the image formation model.

TABLE III
RESTORATION OF THE ZEBRA IMAGE. THE SNR'S OF CHANNEL 1, 2, AND 3 ARE 30 dB, 40 dB, AND 50 dB, RESPECTIVELY

Mean Square Error			
	Channel 1	Channel 2	Channel 3
Without Restoration	19.24	20.38	21.56
Independent	13.61	12.34	10.27
Multichannel	8.13	7.52	7.33

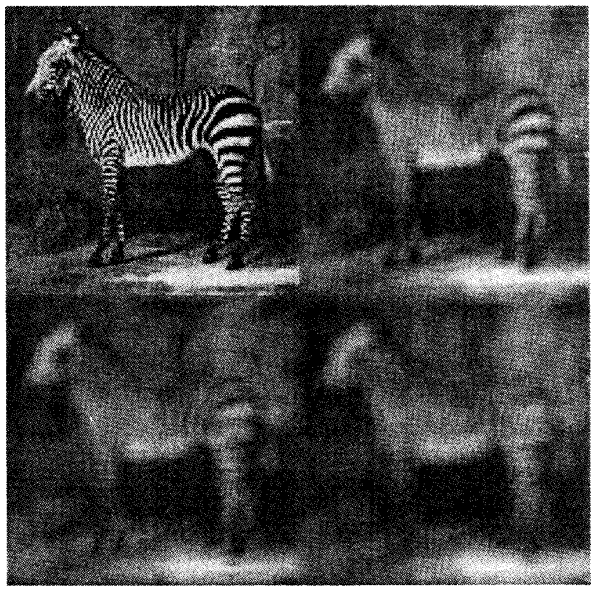

(a)

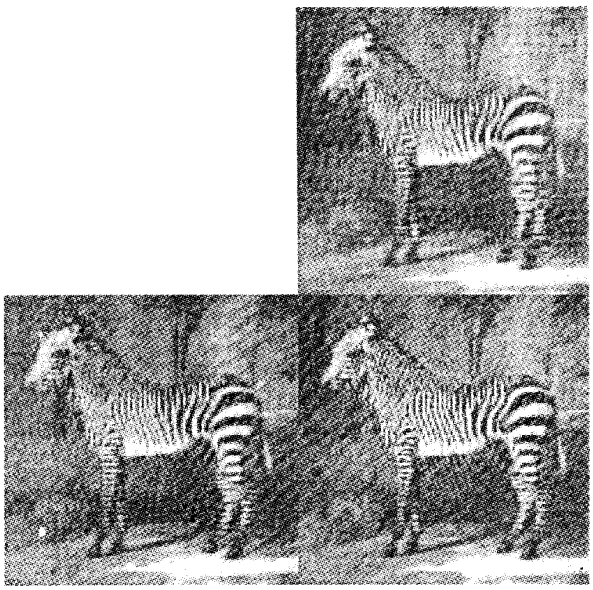

(b)

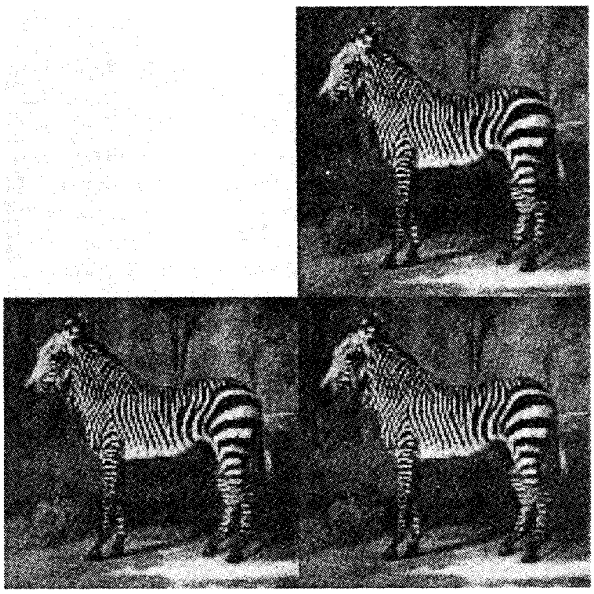

(c)

Fig. 3. (a) Original (upper left) and distorted images of channel 1 (upper right), channel 2 (lower left), and channel 3 (lower right). (b) Independently restored images of channel 1 (upper right), channel 2 (lower left), and channel 3 (lower right). (c) Multichannel restored images of channel 1 (upper right), channel 2 (lower left), and channel 3 (lower right).

The correlation was estimated by

$$R_f^{il}(j, k) = \frac{1}{M^2} \sum_{n=1}^{M} \sum_{m=1}^{M} g_i(j + n, k + m)\, g_l(n, m) \tag{4-3}$$

where $R_f^{il}(j, k)$ is the correlation at position (j, k) between channels i and l. The signals g_i and g_l are the observed image from channel l, respectively. In this case, the estimation used the observed image $\boldsymbol{g}$ instead of the ideal signal $\boldsymbol{f}$. Next, the estimated correlation, the observed signal, and the degradation functions were input to the multichannel restoration scheme and the results were tabulated in Table III. The resulting images are shown in Fig. 3. Again, the multichannel restoration performed better than the independent restoration.

V. Conclusions

This paper presents a computationally feasible algorithm to solve for the Wiener solution (LMMSE) of a multichannel imaging system. Solving for the Wiener solution directly as stated in (2-8) requires N^2M^6 operations for the inversion of (2-9), where N is the number of channels and $M \times M$ is the size of the image. Using the proposed multichannel restoration algorithm as defined in (3-6), the required number of operations for the inversion is reduced to $N^2M^2 \log_2 M$. For large M, for example, 128×128 three-channel images, the difference is significant (10^{14} versus 10^6). Simulations were performed to test the proposed algorithm. It was verified that the multichannel algorithm outperforms the independent restoration.

References

[1] B. R. Hunt and O. Kübler, "Karhunen-Loève multispectral image restoration, Part I: Theory," *IEEE Trans. Acoust., Speech, Signal Processing*, vol. ASSP-32, pp. 592-599, June 1984.

[2] B. R. Hunt, "The application of constrained least squares estimation to image restoration by digital computer," *IEEE Trans. Comput.*, vol. C-22, pp. 805-812, Sept. 1973.

[3] H. C. Andrews and B. R. Hunt, *Digital Image Restoration*. Englewood Cliffs, NJ: Prentice-Hall, 1977.

[4] R. M. Gray, "On the asymptotic eigenvalue distribution of Toeplitz matrices," *IEEE Trans. Inform. Theory*, vol. IT-18, pp. 725-730, Nov. 1972.

[5] N. Kalouptsidis, D. Manolakis, and G. Karayannis, "A family of computationally efficient algorithms for multichannel signal processing—A tutorial review," *Signal Processing*, vol. 5, pp. 5-19, 1983.

Nikolas P. Galatsanos (S'88) was born in Athens, Greece, in 1958. He received the Diploma in electrical engineering from the National Technical University of Athens, in 1982 and the M.S.E.E. degree from the University of Wisconsin-Madison in 1984.

At present he is a Ph.D. candidate in the Department of Electrical and Computer Engineering at the University of Wisconsin-Madison. His research interests include digital image processing, VLSI for digital signal processing, and neural networks applications.

Mr. Galatsanos is a member of the Technical Chamber of Greece.

Roland T. Chin (S'75-M'79) received the B.S. degree with honors in 1975 and the Ph.D. degree in 1979, both in electrical engineering from the University of Missouri, Columbia.

From 1979 to 1981 he was with Business and Technological Systems, Inc., MD, where he engaged in research in remote sensing data analysis and classification for NASA Goddard Space Flight Center, Greenbelt, MD. Since 1981 he has been on the Faculty of the Electrical and Computer Engineering Department at the University of Wisconsin-Madison, where he is currently Associate Professor and Associate Chair. His current research interests include image restoration, texture analysis, shape descriptions, pattern recognition, visual inspection, object recognition, and related applications.

Dr. Chin is a member of Eta Kappa Nu and Tau Beta Pi, and he was the recipient of the First Presidential Young Investigator Award in 1984.